J. Fluid Mech. (1999), *vol.* 394, *pp.* 261–279. Printed in the United Kingdom

On the survival of strong vortex filaments in 'model' turbulence

By ROBERTO VERZICCO[1]† AND JAVIER JIMÉNEZ[2]

[1]Università di Roma 'La Sapienza' Dipartimento di Meccanica e Aeronautica, via Eudossiana n° 18 00184 Roma, Italy

[2]Escuela T. S. Ingenieros Aeronáuticos, Pza. Cardenal Cisneros 3, 28040 Madrid, Spain

(Received 24 July 1997 and in revised form 12 April 1999)

This paper discusses numerical experiments in which an initially uniform columnar vortex is subject to several types of axisymmetric forcing that mimic the strain field of a turbulent flow. The mean value of the strain along the vortex axis is in all cases zero, and the vortex is alternately stretched and compressed. The emphasis is on identifying the parameter range in which the vortex survives indefinitely. This extends previous work in which the effect of steady single-scale non-uniform strains was studied. In a first series of experiments the effect of the unsteadiness of the forcing is analysed, and it is found that the vortex survives as a compact object if the ratio between the oscillation frequency and the strain itself is low enough. A theoretical explanation is given which agrees with the numerical results. The strain is then generalized to include several spatial scales and oscillation frequencies, with characteristics similar to those in turbulent flows. The largest velocities are carried by the large scales, while the highest gradients and faster time scales are associated with the shorter wavelengths. Also in these cases 'infinitely long' vortices are obtained which are more or less uniform and compact. Vorticity profiles averaged along their axes are approximately Gaussian. The radii obtained from these profiles are proportional to the Burgers' radius of the r.m.s. (small-scale) axial strain, while the azimuthal velocities are proportional to the maximum (large-scale) axial velocity differences. The study is motivated by previous observations of intense vortex filaments in turbulent flows, and the scalings found in the present experiments are consistent with those found in the turbulent simulations.

1. Introduction

In the last decade there has been an increasing interest in the strong coherent vortices ('worms') which are found among the small scales of many turbulent flows. Numerical simulations (Siggia 1981; Vincent & Meneguzzi 1991; Jimenez *et al.* 1993 and references therein) and laboratory experiments (Douady, Couder & Brachet 1991; Villermaux, Sixou & Gagne 1995) have shown that these vortices can be traced over lengths comparable to the integral scale of the flow (L_e), although Jiménez & Wray (1998) find that they contain shorter substructures with lengths of the order of the Taylor microscale λ. Their radii are of the order of the Kolmogorov scale η, and their circumferential velocities are of the order of the r.m.s. velocity fluctuations u'. They have lifetimes of the order of the eddy turn-over time of the

† Present address: Politecnico di Bari, Istituto di Macchine ed Energetica, via Re David, 200, 70125 Bari, Italy.

large turbulent scales $T_e = L_e/u'$, which are also implied by their length. A recent survey of their properties, including results from experimental observations at high Reynolds numbers, is Jiménez (1998), which confirms those scalings.

They are therefore very elongated objects, since $\lambda/\eta = Re_\lambda^{1/2}$ and $L_e/\eta \sim Re_\lambda^{3/2}$, where $Re_\lambda = u'\lambda/\nu \gg 1$. Their vorticity, $O(u'/\eta)$, is much higher than the r.m.s. vorticity over the bulk of the flow, ω', and they can therefore only be created by stretching pre-existing structures. Their radius is compatible with this explanation, since the strains available in the background are $O(\omega')$ and can stretch a vortex until its radius is of the order of the Burgers' limit $(\nu/\omega')^{1/2} \sim \eta$. They are however too long for this simple model. A straightforward consideration of the Kolmogorov spectrum shows that the correlation length of any velocity gradient, taken over the bulk of the flow, is of the order of η. This was shown by Jimenez & Wray (1994*b*) to be also the case for the stretching along the worm axes, $\sigma = \boldsymbol{\omega S \omega}/\omega^2$, and is much shorter than the length of the observed filaments. The same paper shows that not only the length scale of σ, but its magnitude and p.d.f. are essentially the same along the axes of the worms as in the bulk of the flow, with compressive and stretching segments of roughly comparable lengths.

There are therefore several levels of organization along the worms axes, on none of which can they be considered uniformly stretched vortices. They are coherent over lengths of $O(\lambda)$, and retain enough structure over the longer scale $O(L_e)$ that they can be recognized as single objects by most tracking algorithms. Over those lengths they are subject to a more or less random stretching which is of $O(\omega')$, but which is only coherent over the much shorter length scale $O(\eta)$, and which is partially compressive. We have seen that their radii are compatible with strains of the order of ω', even if the mean stretching over the longer distance cannot be higher than $O(u'/L_e) \ll O(\omega')$.

A related observation is that the filaments are essentially stable, since their observed lifetimes, $O(T_e)$, are much longer than their internal rotation times $\eta/u' \sim T_e Re_\lambda^{-3/2}$. This can be qualitatively explained because their vorticity is much stronger than the velocity gradients in the surrounding flow, which they see as small perturbations. An isolated axisymmetric columnar vortex is linearly stable, although it supports neutral waves. It becomes unstable when subject to a non-axisymmetric external strain, but the eigenvalues of the instability are only of the order of the imposed strain (Saffman 1992), and the perturbation will not grow unless the forcing maintains roughly the same orientation over times comparable with the inverse of the growth rates. Incoherent turbulent fluctuations have lifetimes which are of the order of the inverse of their velocity gradients, and are therefore unlikely to force the breakdown of a strong vortex.

A related breakdown mechanism was proposed by Miyazaki & Hunt (1998), who studied the interaction of an initially straight vortex with weaker turbulence. They observe the production of linear non-axisymmetric waves on the vortex, and conjecture that they could resonate with the self-induced motion of the turbulent fluctuations. That is unlikely in the case of the filaments observed in the isotropic simulations. The resonance requires the celerity of the axial waves to be similar to the self-induced velocity of the turbulent structures. The former is of the order of $\omega_0 r_0$, where ω_0 is the characteristic vorticity of the core and r_0 its radius. The important perturbations are those near the vortex, which interact among themselves across distances of $O(r_0)$ and which, to have self-induced velocities of the same order as the wave celerity, would need vorticities comparable to those of the core. Thus, while a vortex can be

destroyed by another one of the same intensity, that is unlikely to happen in the interaction with weaker perturbations.

While these arguments may explain why the vortices survive for long times, they do not explain how such long coherent structures form in the first place. There is numerical evidence for the formation of short vortices by rolling of pre-existing vortex sheets (Vincent & Menneguzzi 1994; Passot *et al.* 1995) but, in explaining how those vortices attain the lengths of the observed structures, that mechanism runs into the coherence problems mentioned above. Since the observed radii are of the order of the Burgers' limit for ω', the weak strains which are coherent over scales of the order of L_e are not strong enough to stretch them to the observed radii, while the stronger strains of $O(\omega')$ are not coherent enough to explain the observed lengths.

Jiménez & Wray (1994*a*) conjectured that the mechanism for the formation of long vortices in the presence of essentially incoherent zero-mean stretching is the presence of Kelvin waves travelling along the vortex axes, which tend to smooth the effect of the imposed strain. The proposal was that short strong vortices form with lengths of the order of the incoherent background scales, possibly by roll-up, and are then fused together by the axial waves. They also showed that a consequence of this model is that the vortices cannot be stretched by an inhomogeneous strain beyond the point in which their azimuthal velocity is of the same order as the maximum velocity difference in the driving flow, independently of the vortex circulation and of the strain magnitude. The first mechanism addresses the difficulty of having vortices much longer than the characteristic scale of the stretching strain, while the second observation explains why the velocity p.d.f.s are not intermittent (Anselmet *et al.* 1984) since, contrary to what happens to the vorticity of a stretched vortex, the velocity difference is never amplified.

The formation of nonlinear axial waves in perturbed vortices had already been studied by Lundgren & Ashurst (1989) and Melander & Hussain (1994), among others. Verzicco, Jiménez & Orlandi (1995, from now on referred to as VJO) contains a more complete list of references on the subject prior to 1994. Most of them focus on the importance of the waves in the breakdown of the vortices. Schoppa, Hussain & Metcalfe (1995), for example, propose them as a possible route for small-scale generation inplane mixing layers, and the intent is the same in Melander & Hussain (1993), Marshall (1997) and Miyazaki & Hunt (1998).

Moore & Saffman (1972), on the other hand, mentioned the possibility of homogenization by axial waves as a reason to study the behaviour of uniform vortex cores, and Villasenor & Vincent (1992), analysing the simulations in Vincent & Meneguzzi (1991), mention that short precursor vortices are occasionally connected to longer ones by what appears to be axial waves. Andreotti, Douady & Couder (1998) have recently observed the homogenization of axial stretching in the core of strong vortices, and Hagen & Kurosaka (1993) proposed that axial flows induced by inhomogeneity of the cores of hairpin vortices could be important in the transport of momentum in boundary layers.

VJO were the first to demonstrate a detailed mechanism by which axial waves in viscous vortices could act as a stabilizing effect, and to investigate the range of parameters for which the vortex survives indefinitely. The driving strains that they used were, however, steady and with a simple sinusoidal axial structure, and some details of the survival mechanism seemed to be dependent on the simple structure of the external perturbations.

The homogenization of the axial strain was, for example, traced to the formation of a steady separation bubble at the plane of maximum compression and, since

separation is a notoriously unstable process, it it was not clear whether the same mechanism would act under more general perturbations, such as those likely to be found in turbulence.

Another doubtful point was the mechanism limiting the loss of vortex circulation to infinity. In the compressive regions the vortex thickens, and the vortex lines are carried away from the axis. In an inviscid situation they would reach infinity and the vortex would eventually lose all its circulation in this way. It was argued in VJO that this is prevented by viscous cancellation between vortex sheets of opposite (radial) sign which are advected along neighbouring outgoing streamlines. It was not clear whether this process would survive in unsteady situations in which, in contrast to the steady case, all the points along the axis are under compression at one time or another. It will indeed be seen below that this is not always the case, and that some unsteady conditions result in vortex disintegration, but that there are parameter ranges for which the vortex survives indefinitely.

The purpose of the present paper is to extend the experiments in VJO to unsteady multiscale strains, still with zero axial mean, and to set the limits in which approximately uniform compact vortices survive indefinitely under such strains. One important goal is to clarify, within the necessarily simple strain distributions that can be used in high-resolution simulations, the scaling of the mean vortex radius and azimuthal velocity. It has been mentioned above that the filaments in turbulent flows have radii which correspond to the Burgers' limit of the applied r.m.s. stretching, and azimuthal velocities of the order of the applied r.m.s. velocity difference. These two properties are associated in turbulence with different length scales. While the gradients are highest at the Kolmogorov scale, the velocity differences occur over lengths which are at least $O(\lambda)$ but which, on the average, are $O(L_e)$. This separation of scales could not be investigated using the single-scale simulations in VJO, and the present experiments are designed to test it.

The organization of this paper is as follows. The next section describes the set-up for the numerical experiments, together with the run parameters and the convergence checks. In § 3 the results are discussed, considering first the unsteady single-scale strains and then the multiscale ones, followed by closing remarks in § 4.

2. Numerical set-up

2.1. *Numerical scheme*

The simulations are performed by solving numerically the axisymmetric time-dependent Navier–Stokes and continuity equations for an incompressible viscous flow. The numerical method is that described in Verzicco & Orlandi (1996) with the extensions of VJO to include the effect of an external strain. The main points are the following: the equations, in primitive variables, are discretized on a staggered grid by central second-order finite-difference approximations that conserve the energy in the inviscid limit. The resulting system of equations is solved by the fractional-step method. The advancement in time uses a low-storage third-order Runge–Kutta scheme (A. Wray, personal communication) with the nonlinear terms computed explicitly and the viscous terms implicitly, to avoid the viscous stability limit.

VJO gave the expression for an axisymmetric irrotational strain with zero spatial average, and with a simple sinusoidal behaviour along the x-axis. We use here more general forcings which can be expressed as sums of those single-scale fields, and which

are allowed in general to oscillate in time. The axial strain has the expression

$$s(r,x,t) = \partial_x u = -\sum_{i=1}^{N_S} S_i I_0(\kappa_i r)\sin(\kappa_i x)\sin(f_i t), \tag{2.1}$$

where N_S is the number of axial scales and I_0 is the modified Bessel function of the first kind. S_i is the maximum axial strain at the axis ($r = 0$) associated with the wavenumber $\kappa_i = 2\pi/\ell_i$, and f_i is its oscillation frequency.

Note that, for $r \ll \ell_i$, $I_0(\kappa_i r) \simeq 1 + O(\kappa_i r)^2$, and (2.1) describes a time-dependent strain which is uniform in the radial direction but non-uniform along the axis, and which has zero axial average. As $r \to \infty$ the strain grows exponentially, making (2.1) unphysical and complicating the numerical treatment. In a real turbulent flow such strains would be generated by distributions of azimuthal vorticity away from the axis, which are not included here to focus the attention on the dynamics of the axial vortex. If $\kappa_i \to 0$ the velocity of one summand in (2.1) tends to $u_i = S_i x \sin(f_i t)$ and $v_i = S_i r^2 \sin(f_i t)/2$, and approximates a uniform axisymmetric strain oscillating in time.

The axisymmetry of the forcing strain and of the code are the strongest assumptions in this paper, and it is probably true that sufficiently asymmetric perturbations would lead to different results. The problem that we are trying understand, however, is how the filaments can form and survive under partially compressing situations, in which it appears at first sight that they should break down. We are especially interested in how they achieve a mean radius which is corresponds to the r.m.s. of the strain strain, rather than to its mean. All these are axial effects, only related to the triaxial nature of the perturbations inasmuch as the latter can lead to vortex breakdown, which we have argued in the Introduction to be unlikely. In fact, some non-axisymmetric initial conditions were tried in VJO, without any obvious difference in the final results.

There is moreover evidence that a strong vortex might lead to some symmetrization of the local turbulence. Melander & Hussain (1993) showed that a columnar vortex immersed in an initially turbulent flow field wraps the small-scale turbulence around the core and this process results in the generation of a periodic array of vortex rings of alternating sign surrounding the core. Similar results were recently obtained by Miyazaki & Hunt (1998) who investigated the structure of turbulence around a columnar vortex using rapid distortion theory. In view of those results Marshall (1997) modelled the effect of turbulence on vortex columns by considering coaxial counter-rotating axisymmetric vortex rings whose induced strain field, in its spatial structure, is very similar to (2.1). The main difference with those cases is that we treat stronger vortices, and put the emphasis on finding parameter ranges in which vortices survive, rather than being destroyed.

2.2. *Initial and boundary conditions*

The initial condition is a uniform vortex with a Gaussian axial vorticity distribution

$$\omega_x(r,x) = \frac{\Gamma}{\pi r_0^2}\,\mathrm{e}^{-(r/r_0)^2}, \tag{2.2}$$

where Γ is the circulation of the vortex and r_0 its radius. The initial velocity field is found by adding the azimuthal velocity due to this vortex to the axially periodic irrotational velocity induced by (2.1). The resulting field is axially periodic with the same wavelength as (2.1), and the computation retains this spatial periodicity.

In this paper the circulation is always $\Gamma = 1$ and the initial radius is $r_0 = \frac{1}{2}$. The former is an arbitrary normalization, but the latter implies a particular initial condition, since the length scale is already defined by the axial wavelength. Also problematic is the assumption that the initial vortex is already a uniform connected filament, but the problem of filament formation has already been discussed in the Introduction, and the independence of the final state from the initial conditions was extensively checked in VJO. In the present case, some simulations were performed in which a background vorticity (uniform, non-uniform or with a random distribution) was superimposed onto the columnar vortex (2.2). In all the cases, the final state was found to depend only on the net circulation of the initial field.

The computational domain is axially periodic but finite in the radial direction. The conditions imposed at the outer boundary are that the axial and radial velocities are those of the irrotational strain (2.1), while the azimuthal component satisfies that the axial vorticity vanishes. The position of the outer boundary is a compromise between the need of avoiding artificial effects due to the boundary condition and the constraints imposed on the stability of the code by the exponential growth of the irrotational velocity at infinity. Locating the boundary too far from the axis implies the use of time steps which are uneconomically small, while locating it too near leads to errors that manifest themselves as a loss of circulation. A reasonable compromise was found in VJO to be $R = 4$, and it is the one used here. The conservation of the total circulation was checked in all the simulations as an indicator of the quality of the results.

2.3. *Run parameters*

The flow is characterized by two dimensionless parameters: an azimuthal Reynolds number $Re_\Gamma = \Gamma/\nu$, based on the vortex circulation, and a longitudinal one, $Re_\ell = S\ell^2/\nu$, based on the forcing strain and on its axial length scale. For a purely sinusoidal forcing there is no ambiguity in the definition of S and ℓ. VJO used the amplitude of (2.1) and its wavelength. Here it was found convenient to use the maximum strain S_{max} generated at the axis by (2.1), and the length $\ell = \pi\Delta u_x/S_{max}$, defined in terms of the maximum velocity difference Δu_x induced by (2.1) along the axis. For a single-scale forcing they are equivalent to the older definitions. Their physical significance is that an $O(S)$ strain generates axial velocity differences which are $O(S\ell)$.

We have already noted that the exponential radial behaviour of the driving velocity is essentially artificial, but it produces unnecessary complications in the dynamics whenever the vorticity is transported to large distances from the axis. It was shown by VJO that the effect of this radial structure is negligible provided that the ratio $Re_\Gamma/Re_\ell > 10$, and the present simulations use parameter combinations beyond that threshold.

A first set of simulations is run with unsteady single-scale forcing, $N_S = 1$, to investigate the effect of the unsteadiness on the core dynamic. The wavelength in all these cases is $\ell = 6$, and the other run parameters are given in table 1. The numerical grid used in these simulations is 128×128, similar to the ones in VJO, where grid independence was established.

A second set of simulations is run using steady two-scale forcing, $N_S = 2$, to simulate conditions closer to real turbulence. In those cases the parameters are chosen so that the strain associated with the shorter wavelength is higher than that associated with the longer one, while the opposite is true for the velocities, $S_i\ell_i$. This is intended to mimic the velocity spectrum of turbulent flows.

Case	S	Re_Γ	P	f/S	Comment
1	0.3947	25	3.530	0.050	d
2	0.3947	25	3.530	0.202	d
3	0.3947	25	3.530	0.506	d
4	0.3947	50	5.604	0.050	d
5	0.3947	50	5.604	0.506	d
6	0.3947	71	7.059	0.250	o
7	0.3947	75	7.343	0.500	d
8	0.3947	100	8.895	0.050	o
9	0.3947	100	8.895	0.202	o
10	0.3947	176	13.000	0.400	o
11	0.3947	200	14.120	0.250	o
12	0.3947	200	14.120	0.500	o
13	0.3947	200	14.120	1.000	d
14	0.3947	400	22.414	0.500	o
15	0.3947	400	22.414	0.750	d
16	0.7895	75	5.827	0.500	d
17	0.7895	82	6.200	0.100	d?
18	0.7895	94	6.800	0.100	o
19	0.7895	100	7.059	0.250	o
20	0.7895	114	7.700	0.375	d?
21	0.7895	120	8.000	0.500	d
22	0.7895	150	9.250	0.250	o
23	0.7895	150	9.250	0.375	o
24	0.7895	168	10.000	0.625	d
25	0.7895	200	11.206	0.250	o
26	0.7895	200	11.206	0.375	o
27	0.7895	200	11.206	0.500	o
28	0.7895	235	12.500	0.500	d
29	0.7895	250	13.000	0.375	o
30	0.7895	300	14.685	0.250	o
31	0.7895	300	14.685	0.500	o
32	0.7895	300	14.685	0.625	d
33	0.7895	300	14.685	0.750	d
34	0.7895	400	17.789	0.500	o
35	0.7895	400	17.789	0.625	d

TABLE 1. Run parameters for the cases with oscillating non-uniform strain. The comment 'd' means that the vortex diffuses, 'o' that it survives, and the 'd?' notation in 17 and 20 marks cases where it is not clear whether the vortex survives or decays very slowly. The parameter $P = Re_\Gamma / Re_\ell^{1/3}$ is discussed in § 3.1.

In a last set of simulations the two-scale forcing is made unsteady, with the oscillation frequencies chosen so that the shorter wavelengths oscillate faster. This again mimics real turbulence, although no effort is made to simulate quantitatively the $k^{-5/3}$ spectrum. The parameters of these last two sets of simulations are given in table 2. It is found necessary in some cases to increase the axial domain length to accommodate the higher aspect ratios of the multiscale forcing. In those cases the number of grid points in the axial direction is increased to maintain the same numerical resolution as in the single-scale cases discussed above. Strains with $N_S > 2$, or having a larger scale ratio than those in table 2, are made numerically impractical by the exponential behaviour of the velocities away from the axis.

Case	Re_Γ	S_1	S_2	ℓ_1	ℓ_2	f_1/S_1	f_2/S_2	P	f_{max}/S_{max}	Comment
1	70	0.13	0.53	15	3	0	0	6.43	0	—
2	100	0.44	0.53	6	3	0	0	9.87	0	—
3	100	0.39	0.53	12	3	0	0	6.56	0	—
4	100	0.20	0.53	12	3	0	0	8.20	0	—
5	168	0.13	0.53	15	3	0	0	11.52	0	—
6	100	0.30	0.60	6	3	0.20	0.3	10.44	0.20	o
7	100	0.30	0.60	9	3	0.20	0.3	7.63	0.20	o
8	100	0.23	0.49	16	4	0.20	0.3	6.46	0.20	o
9	100	0.23	0.49	16	4	0.50	0.8	6.46	0.54	d
10	200	0.23	0.49	16	4	0.35	0.5	12.26	0.34	o
11	300	0.23	0.49	16	4	0.35	0.5	13.45	0.34	o
12	400	0.11	0.25	16	4	0.35	0.5	20.56	0.34	o
13	400	0.23	0.49	16	4	0.35	0.5	16.25	0.34	o

TABLE 2. Run parameters for the cases with multiscale steady and oscillating strains. S_{max} and ℓ are defined in § 2.3 and f_{max} is the highest of the two frequencies.

3. Results

Before discussing the results of an unsteady external forcing we will briefly recall the behaviour found in VJO for a steady non-uniform strain. The vortex reacts to the inhomogeneity by creating axial currents (Kelvin waves) whose effect is to locally reverse the sign of the forcing, making the vortex survival possible even where it is compressed. This process only works if the vortex is intense enough, and is quantitatively described by the parameter $P = Re_\Gamma / Re_\ell^{1/3}$, which separates the core dynamics into three distinct regimes. For $P \leqslant P_I \approx 6$ the vortex is compact in those places where it is stretched by the external strain, and bursts where it is compressed. In this regime the axial waves do not form or are weak, and the axial strain maintains the same sign at the axis as away from it. The maximum vorticity and azimuthal velocity increase with Re_Γ roughly as they would for a uniform Burgers' vortex. For $P_I < P \leqslant P_{II} \approx 12$ the axial waves are strong enough to reverse locally the sign of the compressive strain. This creates a separation bubble centred on the compressed part of the vortex which, as P increases, becomes longer and fills the whole axis when $P \simeq P_{II}$. The reversal process of the strain is complete for $P > P_{II}$, and the flow becomes basically independent of the Reynolds number. In this regime the maximum vorticity at the axis, normalized by $SRe_\ell^{1/3}/4\pi$, becomes independent of P (see figure 5*b*).

This classification applies to the final steady state of the flow. When the forcing is applied to an initially cylindrical vortex there is a transient phase during which the separation bubble is generated, spreads along the vortex axis, and eventually reverses the sign of the compressive strain.

3.1. *Unsteady forcing*

In the unsteady case, the situation is complicated because, when the external strain changes, the effect of the axial waves depends on how fast they can form and react. This is shown in figure 1, where the meridional stream function and the axial vorticity are shown at several phases of the oscillation cycle. The instantaneous structure of the strain on the axis is shown to the right of each frame, and it is clear that the formation of the separation bubble lags behind the forcing. For example, the strongest separation does not happen in panel (*a*), when the compressive strain is maximum,

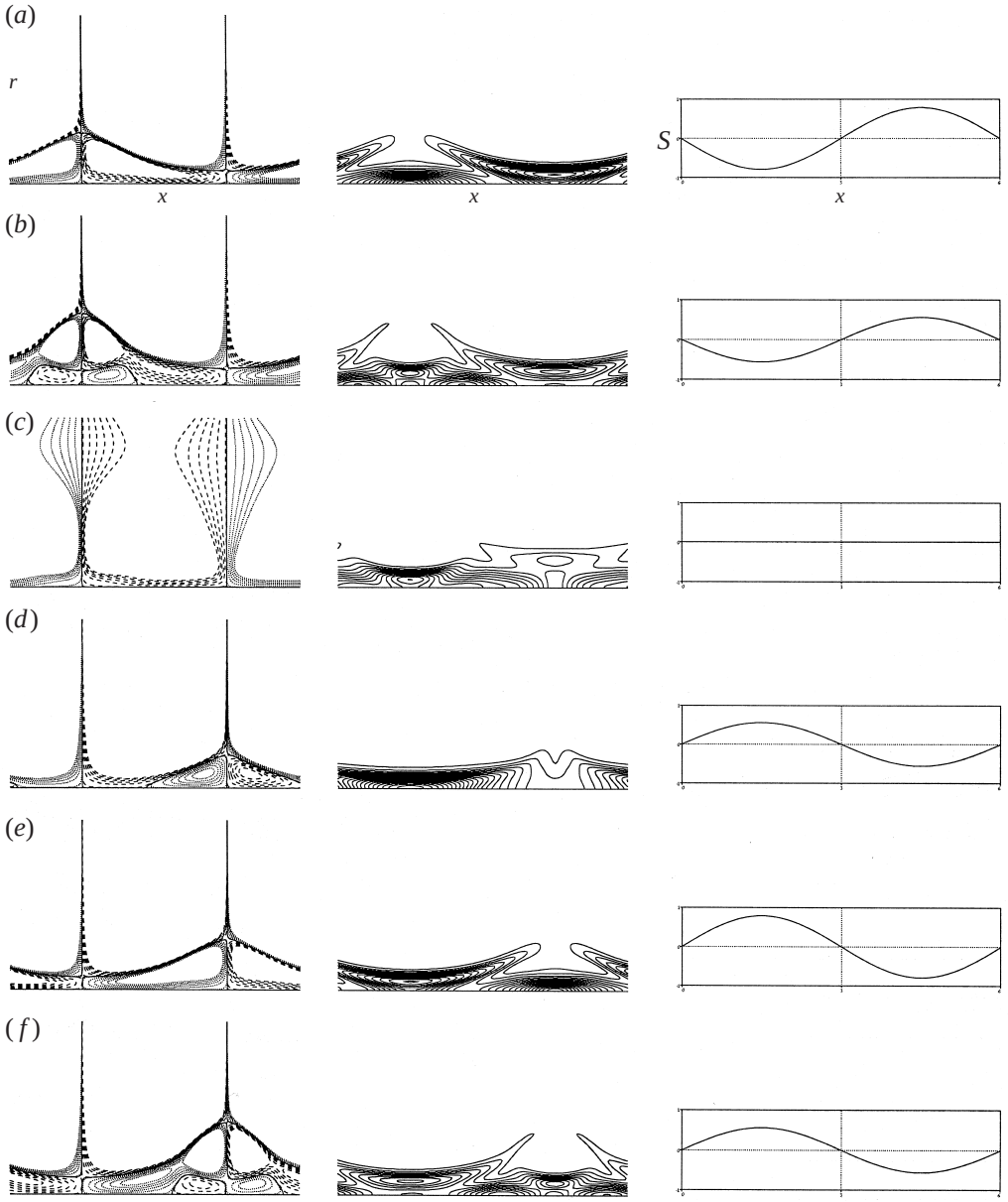

FIGURE 1. Meridional streamlines (left column) and axial vorticity (centre) for case 25 of table 1: (*a*) $t = 0$, (*b*) $T/8$, (*c*) $2T/8$, (*d*) $3T/8$, (*e*) $4T/8$, (*f*) $5T/8$. Stream function: ·····, negative values; – – –, positive; ———, $\psi = 0$. $\Delta\psi = 0.009$. Only the values up to $|\psi| = 0.046$ are plotted. Vorticity: $\Delta\omega = \pm 0.2$. The instantaneous strain at the axis is shown to the right of each frame.

but in (*b*), when the strain is already decreasing. It follows that the survival of the vortex depends on the relation between the formation time of the waves and the forcing frequency. If the oscillation of the external strain is too fast, the waves do not have time to form, and each section of the vortex 'feels' a spatially uniform oscillating strain. Lundgren (1982) gave a general solution for the evolution of vortices in a

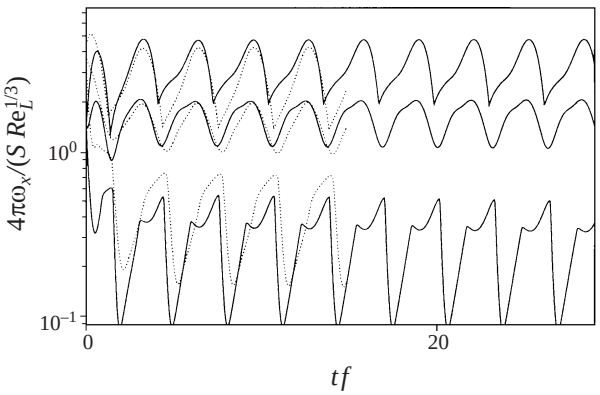

FIGURE 2. Evolution of the maximum, minimum and average vorticity at the axis, for cases 6 (———) and 19 (·····) in table 1, scaled as in VJO.

uniform axial strain. In our case, in which the mean stretching is zero, it implies that the radius of the vortex increases asymptotically as $t^{1/2}$ and that its vorticity decays as $\omega_0 \sim t^{-1}$, as in the case of pure viscous diffusion. This behaviour is found here, for example, in figures 3(*a*), 3(*c*) and 7(*b*).

The essence of the argument in VJO was that the magnitude of the strain generated by the vortex reaction is of the order of

$$S_w = \frac{\Gamma Re_\ell^{2/3}}{\ell^2} = SP, \tag{3.1}$$

which suggests that the formation time of the separation bubble is of order S_w^{-1}, and that the importance of the unsteadiness should be measured either by f/S, which is the relevant time ratio for the stretching part of the cycle, or by f/SP, which applies during the compressive part. The behaviour of the axial vorticity for two unsteady cases, which were chosen with similar values of f/S and P to check whether the scaling (3.1) still applies in the unsteady case, is shown in figure 2 and agrees reasonably well. A similar check was run between cases 10 and 29 of table 1.

These arguments suggest that the $(f/S, P)$-plane should be divided according to three criteria:

(*a*) Below a 'reaction' threshold, $P < P_I$, the vortices do not survive because the Kelvin waves are not strong enough to counteract the compressive strain, even if given infinite time to act.

(*b*) Above a maximum 'stretching frequency', $f/S \sim 1$, the oscillation is too fast for the vortex to reach equilibrium during the stretching phase of the cycle, and the vortex diffuses.

(*c*) Above a maximum 'compression frequency', $f/S \sim P$, the oscillation is too fast for the reactive strain to develop during the compressive phase of the cycle, and the vortex bursts.

Only within these boundaries is the vortex able to survive.

Note that the previous discussion on time scales could be framed as the interaction of the vortex, seen as a linear damped oscillator, and the external periodic forcing. This approach was for example taken by Miyazaki & Hunt (1998), who speculated that resonance could be responsible for the strong coupling between the two. This is not completely implausible, since we have already mentioned that the basic reaction mechanism by the vortex is the generation of Kelvin waves, which are essentially linear

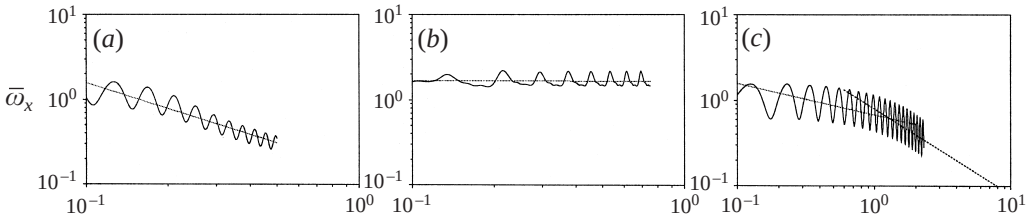

FIGURE 3. Time evolution of the average vorticity at the axis. (*a*) Case 13, (*b*) case 25, (*c*) case 16. ———, Numerical result; – – – –, power law fit.

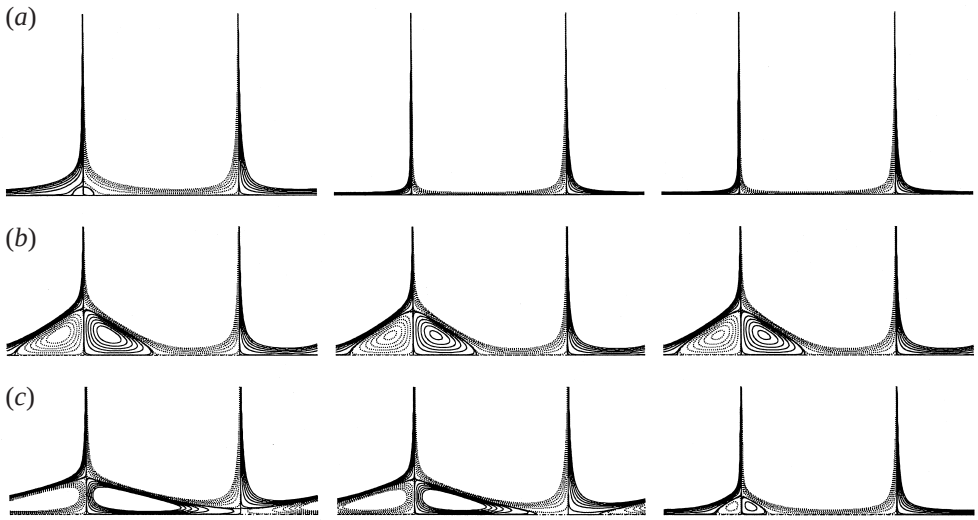

FIGURE 4. Meridional streamlines at $t = T/8$ in the oscillation cycle, for (*a*) case 33; (*b*) 19 and (*c*) 21, table 1. The three columns correspond to the second, third and fifth oscillation cycles. Only the values up to $|\psi| = 0.046$ are plotted: ·····, negative; ———, positive values. $\Delta\psi = \pm 0.009$.

phenomena. It should be clear, however, that the effects that we are describing here are nonlinear. It will be seen below that the description in (*a*)–(*c*) is essentially correct. At large times the vortex either survives intact, or decays completely, and such bimodal behaviours cannot be accounted for by linear models. In the cases in which the vortex survives, its mean radius is not determined linearly, proportional to the mean forcing strain, which is zero, but as a nonlinear function of the oscillating amplitude. It was also shown in VJO that the parameter P, which distinguishes between surviving and decaying vortices, can only be explained by taking into account the finite axial variations of the core radius. Thus, while some vortex interactions can probably be explained by resonant interactions of linear waves, nonlinearity is an intrinsic ingredient of the phenomena described in this paper. It was, in addition, already noted in the Introduction that the perturbations found in turbulent flows, which are the ones of interest here, are too slow to resonate with the fast axial waves associated with the strong cores observed in the direct simulations and in the experiments.

3.2. *Single-scale unsteady forcing*

A convenient way of characterizing the vortex behaviour is to monitor its *average* vorticity at the axis, $\overline{\omega}_x(t) = L^{-1}\int_0^L \omega_x(0,x,t)\,\mathrm{d}x$, which undergoes fast oscillations with frequencies of the order of f, superimposed on a secular trend with a viscous

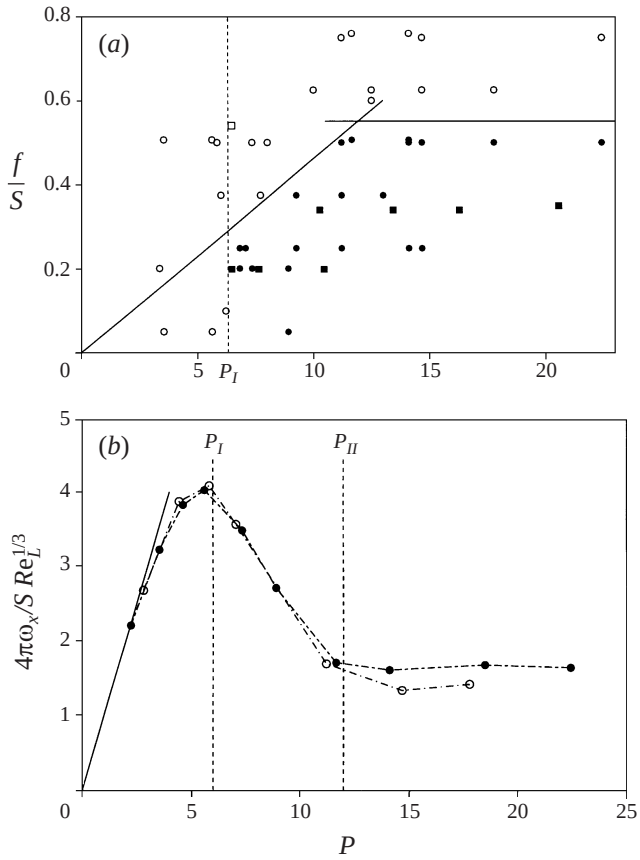

FIGURE 5. (*a*) Vortex behaviour in the plane $f/S, P$: solid symbols mark oscillating cases, open symbols, diffusing ones: ○, single-scale; □, multiscale runs; – – – –, reactive limit; ———, frequency limits. (*b*) Maximum axial vorticity at the axis vs. the local separation parameter for the case of steady, single-scale forcing in VJO: ———, Burger's limit; ○, $Re_\ell/Re_\Gamma = 28.4$; ●, 14.2.

time scale $t_v = t/Re_\Gamma$. The character of the latter defines the survival of the vortex, and the three types of observed behaviour are summarized in figure 3.

(*a*) In some cases the vorticity decays viscously as t_v^{-1}. The plots in figure 4(*a*) show that the streamlines are in this case essentially those of the external forcing and that the presence of the vortex does not affect the meridional flow.

(*b*) For combinations of f/S and P satisfying the three criteria explained above, the vortex survives, and the vorticity is oscillatory. In those cases a separation bubble forms periodically in the compressed regions of the vortex axis, as shown in figures 1 and figure 4(*b*).

(*c*) There are intermediate cases in which the vortex initially diffuses slowly, showing that there is some reaction from the axial waves. But as the axial vorticity gets weaker, so do the waves and, after an initial transient, the t_v^{-1} viscous diffusion dominates (figure 4*c*).

The results of the single-scale simulations are summarized in figure 5(*a*) where it is evident that the vortices survive only in the region of the $(P, f/S)$-plane bounded by the three criteria given above. The corresponding figure for steady strains is reproduced from VJO in figure 5(*b*), and it is clear that the threshold P_I is the same

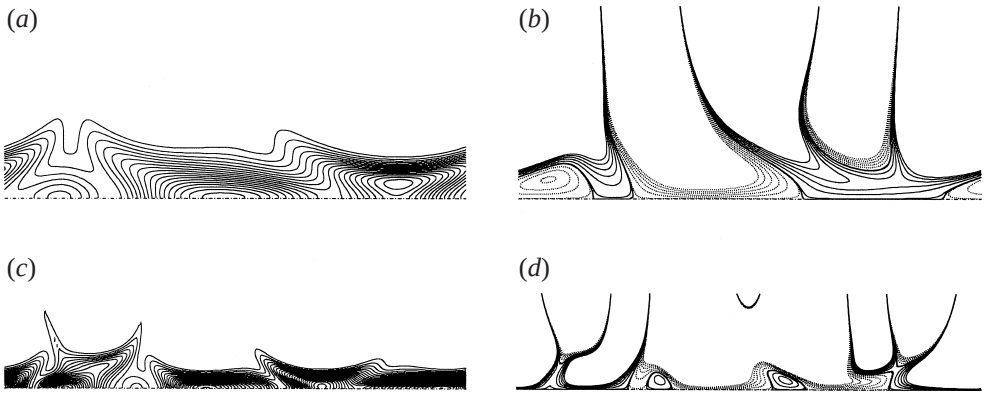

FIGURE 6. Contour plots at the steady state for: (a, b) case 2 and (c, d) 3, table 2. (a, c) are contours of axial vorticity, $\Delta\omega = 0.1$; (b, d) are streamlines, $\Delta\psi = \pm 0.009$.

in both cases. It is also seen from the comparison that the compression and stretching frequency thresholds intersect at a value of P very close P_{II}, which is where the separation bubble spans the whole axis. It is not clear whether this is coincidental, but it is intuitively reasonable that, once the waves are strong enough to induce separation over the whole vortex axis, and their stationary state becomes independent of P, the same should be true for the frequency criterion.

Cases 17 and 20, in which our limited-time simulations cannot distinguish if the vortex survives or decays very slowly, are both close to the boundary of the 'survival region' in figure 5(a).

3.3. *Multiscale forcings*

The results in the previous section show that unsteady non-uniform strains can sustain compact vortices as long as the oscillation frequency is of the same order of magnitude as the strain, as it would be in a turbulent flow. The spatial structure is however still sinusoidal which, as noted in the Introduction, is a poor model for real turbulence and does not allow us to determine properly the scaling behaviours. In this section we discuss the experiments summarized in table 2, in which the driving strain is defined as the sum of two different sine waves. Note that, as discussed in § 2.3, S_i and ℓ_i have been chosen so that the largest strain is associated with the smaller wavelength, while the opposite is true for the velocities, $U_i \sim \ell_i S_i$. The purpose of the experiments in this section is not so much to identify new mechanisms of vortex survival, which will be seen to be essentially the same as in the cases discussed up to now, but to test whether those mechanisms still work in more complex situations. There is therefore no systematic variation of parameters. Instead we use the definitions given in § 2.3 for the global strain and length, and choose parameters inside the 'survival' region identified in the previous section. As a consequence most of our experiments reach a steady state in the form of approximately compact vortices. Case 9 was purposely chosen outside that zone, and it is the only one in which the vortex fails to reach a compact state.

The strains in cases 1–5 are steady, and the simulations are continued until the vortex reaches a steady state. The final flow fields are shown in figure 6 for two examples with different wavelength ratios, and show features which are essentially the same as those found in the simpler cases of the previous section and in VJO. Note that the resulting vorticity distributions, especially in the case with the highest

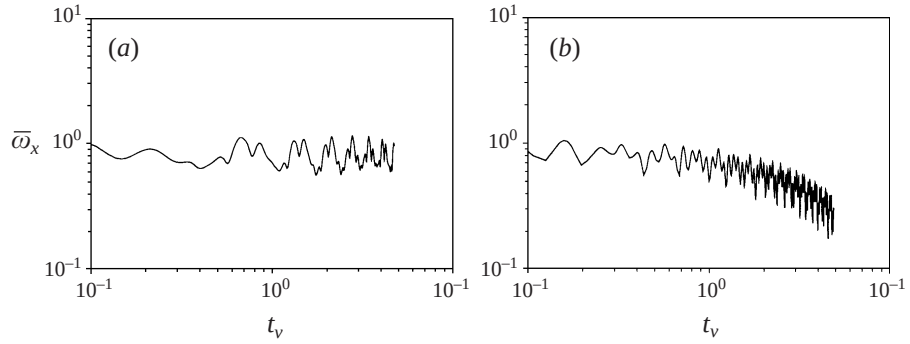

FIGURE 7. Evolution of the average axial vorticity at the axis. (*a*) Case 7, (*b*) 9, table 2.

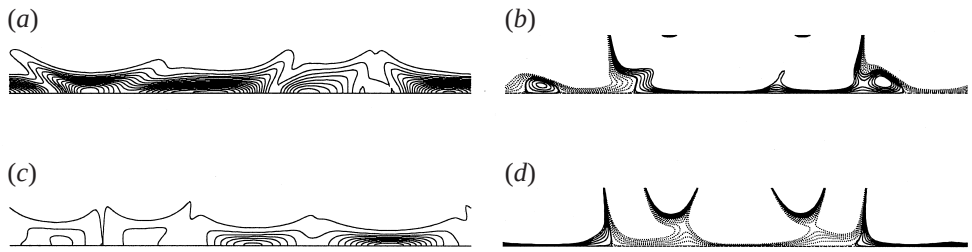

FIGURE 8. Instantaneous contour plots for: (*a*, *b*) case 8 and (*c*, *d*) 9, table 2. (*a*, *c*) are contours of axial vorticity, $\Delta\omega = 0.2$; (*b*, *d*) are streamlines, $\Delta\psi = \pm 0.009$.

wavelength ratio (case 3, $\ell_1/\ell_2 = 4$) would be readily classified as continuous vortices by most identification algorithms. Note also that in this section, as in the previous ones, the averaged strain along the axis is zero.

The remaining cases of table 2 are the most complex experiments in the present set, with strains that are both multiscale and unsteady. Following the results of the previous section, and the motivation from turbulent flows, the oscillation frequency for each harmonic has been chosen as roughly proportional to its strain, but not precisely so. As a consequence, even if the wavelengths of the two components are multiples of each other, the frequencies are not, and the strain distribution varies essentially randomly in time. The best parameter to describe the effect of the unsteadiness was found to be the ratio f_{max}/S_{max}, between the highest frequency and the maximum strain defined in § 2.3. It is given in table 2 and has been used to include these cases in figure 5(*a*). Whenever the effective $f/S, P$ pair is inside the survival zone, the vortex evolves more or less periodically in time and remains compact, with strong axial waves along its axis (see figures 7*a* and 8*a*). On the other hand, when the frequency is chosen too large, the vortex eventually diffuses (figures 7*b* and 8*c*). As in the single-scale case, once this happens the meridional streamlines are essentially those of the external forcing (figure 8*d*), but surviving vortices (figure 8*b*) react to the local compression, forming unsteady separation bubbles.

The vortices that result from this last set of simulations are the ones which are closer to those found in turbulent flows, although the similarity is incomplete. Not only are turbulent vortices not straight and axisymmetric but they are free to orient themselves with respect to the local strain tensor, and the mean stretching is for them slightly positive rather than zero (Betchov 1956).

It is still interesting to compare the statistical properties of the vortices obtained

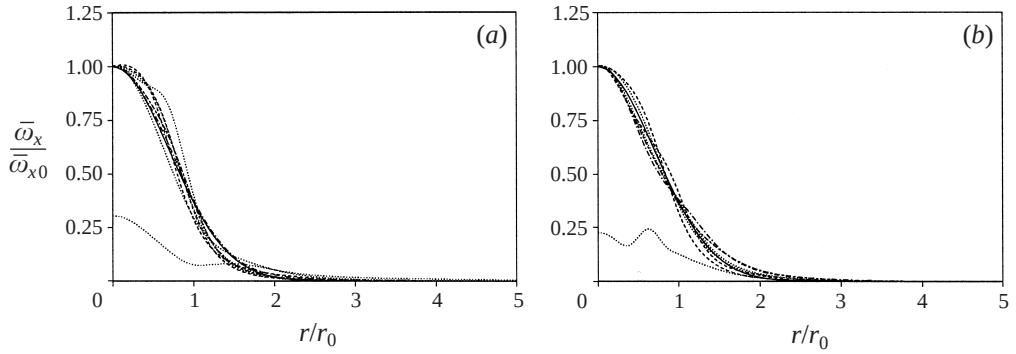

FIGURE 9. Normalized mean radial $\overline{\omega_x}$ profiles for the multiscale cases of table 2: (*a*) steady strain, (*b*) unsteady. The separate dotted lines in each plot are typical profiles of the standard deviations.

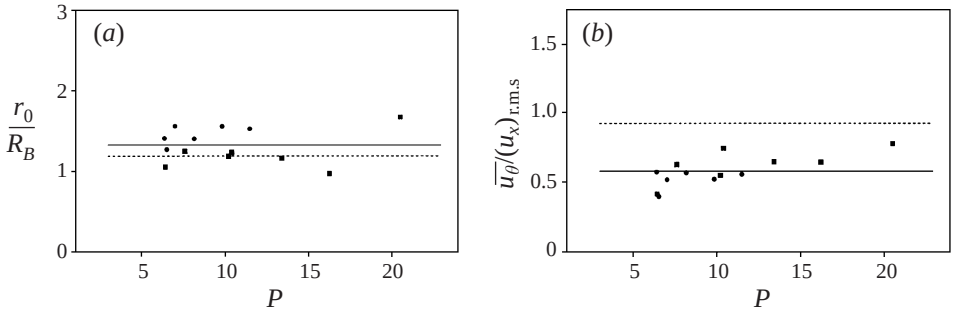

FIGURE 10. (*a*) Mean radius obtained from the vorticity profiles in figure 9 normalized with the Burgers' radius of the r.m.s. strain. (*b*) Mean azimuthal velocity $\overline{u_\theta}$, normalized with the r.m.s. driving axial velocity. ●, Steady; ■, unsteady cases. The solid lines are $r_0/R'_B = 1.31$, and $\overline{u_\theta}/u'_x = 0.58$, which fit the present data, while the dashed ones, $r_0/R'_B = 1.18$ and $\overline{u_\theta}/u'_x = 0.92$, are averages from the turbulence simulations in Jiménez & Wray (1998).

here with those observed in turbulence. It is impractical in the latter case to obtain vorticity maps with a detail comparable to the present ones, but azimuthally and axially averaged vorticity profiles have been published by Jiménez & Wray (1994*b*, 1998). Axially averaged profiles for the multiscale simulations discussed here are given in figure 9. Both the steady and the unsteady cases, but especially the latter, are well approximated by a Gaussian profile, as in real turbulent flows. Figure 9 includes typical profiles of the standard deviation of the vorticity with respect to the mean, which is small. It may be significant that the standard deviations of the unsteady cases are lower than those of the steady ones. In turbulent flows these deviations are still lower ($\simeq 0.1$), consistent with a trend in which more irregular forcings would give rise to smoother vortices.

By fitting the individual profiles in figure 9 to the Gaussian model in (2.2) it is possible to define an average maximum vorticity and radius for each case, which can then be compared to similar fits in Jiménez *et al.* (1993). The results for all the surviving multiscale cases are given in figure 10. In figure 10(*a*) the radius is normalized with the Burgers' radius $R'_B = 2(\nu/S')^{1/2}$, obtained from the r.m.s. strain along the axis. The comparable result in turbulence would be the ratio of the vortex radius to the Burgers' radius based on the r.m.s. value of the axial stretching $\langle\sigma^2\rangle^{1/2}$.

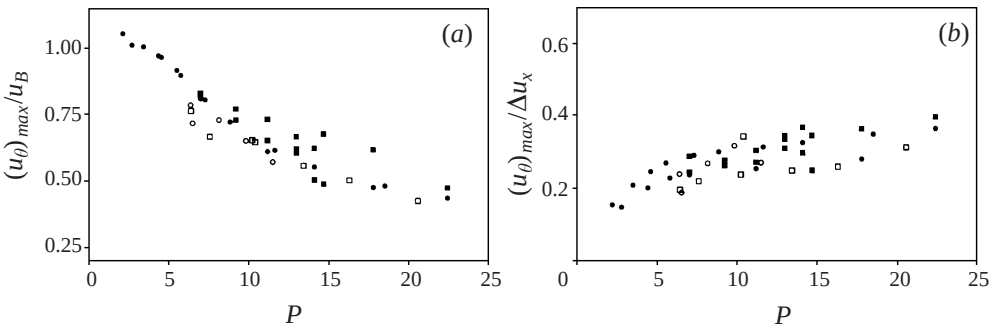

FIGURE 11. Maximum azimuthal velocity vs. separation parameter: (*a*) normalized with the Burgers' velocity, (*b*) normalized with the maximum axial velocity difference. ●, Single-scale steady strain; ■, single-scale unsteady strain; ○, multiscale steady strain; □, multiscale unsteady strain.

The latter is not published for any of the simulations cited in the Introduction, but a re-analysis of the p.d.f.s published by Jiménez & Wray (1994*b*) gives $R/R_B' \approx 1.18$, in reasonable agreement with the values in figure 10.

Another important quantity is the averaged maximum azimuthal velocity in the vortex cores that, for a Gaussian vortex, is approximately $\overline{u_\theta} \approx 0.32\, r_0 \omega_{x0}$. In turbulent flows this quantity is approximately equal to the one-component r.m.s. value of the velocity u' (Jiménez & Wray 1998). The results for the present multiscale simulations are given in figure 10(*b*), where we have used the r.m.s. value of the driving velocity at the axis instead of u'. The result is lower than in the fully turbulent case, but the scaling is the same and the order of magnitude is correct. As previously noted the correspondence of the present experiments with real turbulence cannot be carried too far, and any quantitative result has to be treated with care, but the agreement in scaling behaviour and in order of magnitude is encouraging and supports the claim that the dominant effects are the same in both cases.

A final result is given in figure 11, which includes some single-scale cases and results from VJO, besides the multiscale simulations discussed in this section. The issue to be tested is whether the vortices are indeed globally modified by the axial wave mechanism. The quantity displayed in the figure is the absolute maximum azimuthal velocity found anywhere in a given simulation. If we were dealing with a uniformly stretched vortex, this would be the Burgers' velocity, which is given by the vortex circulation and by the Burgers' radius associated with the maximum stretching strain,

$$u_B \approx 0.32\, \frac{Re_\Gamma}{2\pi} (\nu S_{max})^{1/2}. \tag{3.2}$$

The prediction of the wave-dominated model is that the maximum azimuthal vorticity is proportional to the maximum imposed velocity difference along the axis, since the axial waves do not let the vortex collapse anywhere beyond a radius which is determined globally, rather than locally (Jiménez & Wray 1994*b*; VJO). Both comparisons are made in figure 11 as a function of the separation parameter P. It is clear that, while the Burgers' regime is dominant at low P, where the waves are known to be weak, as soon as $P > P_I$ the Burgers' scaling ceases to apply and the azimuthal velocity is determined globally as a fraction of the driving velocity difference.

4. Conclusions

We have shown that a strong enough vortex core can survive indefinitely in the presence of essentially random axial driving strains, as long as certain parameter ranges are satisfied. We have also shown that, if the vortex survives, its mean radius is determined by the r.m.s. amplitude of the axial strain, rather than by its mean value, so that its length is not limited by the coherence length of the strain, and is essentially infinite. The experiments in this paper were carried out in the extreme case in which the average axial strain is zero, and the axis is therefore approximately evenly divided into stretching and compressive segments.

The study was motivated by the observations of strong coherent vortex filaments in turbulent flows, whose radii are of the order of the Burgers' limit for strains of the order of the r.m.s. velocity gradients over the rest of the flow, but which are much longer than the observed correlation lengths for those gradients. The mean strains over those long distances are much smaller than the r.m.s. value, and observations confirm that the filaments are compressed rather than stretched over a substantial fraction of their length. The model used here, a columnar vortex subject to an alternating strain with global zero average, was suggested by those observations.

The conclusions in this paper generalize similar results in VJO for the simpler case of a steady sinusoidal forcing. In both cases a critical condition for vortex survival is that the ratio

$$P = Re_\Gamma / Re_\ell^{1/3} \tag{4.1}$$

should be large enough. While Re_Γ is unambiguously defined in terms of the vortex circulation, it was not clear from VJO how Re_ℓ was to be defined for more general strains. It is confirmed here that the proper definition is

$$Re_\ell = \pi^2 \Delta u_x^2 / \nu S_{max}, \tag{4.2}$$

where Δu_x is the maximum velocity difference induced by the strain, and S_{max} the maximum strain. Note that the former is a global quantity, while the latter is a local one. In turbulence, where $\Delta u_x \sim u'$ and $S_{max} \sim \omega'$, (4.2) would be proportional to the microscale Reynolds number Re_λ.

Another condition has to be satisfied in the case of unsteady strains. The time scale for the unsteadiness cannot be much shorter than the inverse of the maximum strain. This is clearly true for inertial-range fluctuations in turbulence, where both the strain and the unsteadiness are determined by a single time scale. As before, the present multiscale experiments allow us to define the proper scales to use, which are the fastest oscillation frequency and the strongest pointwise strain.

The theoretical criteria for vortex survival have been related to considerations of the behaviour of axial pressure waves. Those arguments explain all the new observations and are compatible with those in VJO in the steady case. The new experiments, on the other hand, allow us to distinguish between different interpretations of the old criterion, and in particular separate the effects of maximum strain and maximum driving velocity.

The average azimuthal velocity and radius of the vortices subject to complex strains scale with the different flow parameters in a way which is consistent with the behaviour of vortex filaments in turbulent flows, and which agrees quantitatively with them within a factor better than 2. Their lengths, which in the present spatially periodic experiments is essentially infinite, explain the anomalously long lengths observed in the turbulent filaments. We also confirm that the *maximum* azimuthal velocity found in the vortices is bounded by the maximum driving velocity difference,

and is independent of the maximum local stretching and of the vortex circulation. This observation, when translated to the turbulent flow, reinforces the previous claim by Jiménez & Wray (1994*a*) and VJO that the axial wave mechanism is responsible for the lack of intermittency effects in the turbulent velocity, as opposed to the velocity gradients.

It is interesting that the mean vorticity profiles of the driven vortices are approximately Gaussian, even in the presence of extensive unsteady separation along their cores, and that this behaviour, that is also found in turbulent simulations, becomes more marked as the driving strain becomes more complex.

The research was partially supported by CICYT (Spain) under contract PB95-0159, and by grants from 'Ministero dell' Università e della Ricerca Scientifica e Tecnologica', MURST 60% and 40%.

REFERENCES

Andreotti, B., Douady, S. & Couder, Y. 1998 Experimental investigation of the interaction between stretching and vorticity in constrained geometries. In *Advances in Turbulence VII* (ed. U. Frisch), pp. 349–352. Kluwer.

Anselmet, F., Gagne, Y., Hopfinger, E. J. & Antonia, R. A. 1984 High order velocity structure functions in turbulent shear flows. *J. Fluid Mech.* **140**, 63–89.

Betchov, R. 1956 An inequality concerning production of vorticity in turbulence. *J. Fluid Mech.* **1**, 497–504.

Douady, S., Couder, Y. & Brachet, M. E. 1991 Direct observation of the intermittency of intense vortex filaments in turbulence. *Phys. Rev. Lett.* **67**, 983–986.

Hagen, J. P. & Kurosaka, M. 1993 Corewise cross-flow transport in hairpin vortices – The 'tornado effect'. *Phys. Fluids* A **5**, 3167–3174.

Jiménez, J. 1998 Small scale intermittency in turbulence. *Eur. J. Mech.* B/*Fluids* **17**, 405–419.

Jiménez, J. & Wray, A. A. 1994*a* Columnar vortices in isotropic turbulence. *Meccanica* **29**, 453–464.

Jiménez, J. & Wray, A. A. 1994*b* The dynamics of intense vorticity in isotropic turbulence. *CTR Annual Res. Briefs* 1994. Stanford University.

Jiménez, J. & Wray, A. A. 1998 On the characteristics of vortex filaments in isotropic turbulence. *J. Fluid Mech.* **373**, 255–285.

Jiménez, J., Wray, A. A., Saffman, P. G. & Rogallo, R. S. 1993 The structure of intense vorticity in isotropic turbulence. *J. Fluid Mech.* **255**, 65–90.

Lundgren, T. S. 1982 Strained spiral vortex model for turbulent fine structure. *Phys. Fluids* **25**, 2193–2203.

Lundgren, T. S. & Ashurst, W. T. 1989 Area-varying waves on curved vortex tubes with application to vortex breakdown. *J. Fluid Mech.* **200**, 283–307.

Marshall, J. S. 1997 The flow induced by periodic vortex rings wrapped around a columnar vortex core. *J. Fluid Mech.* **345**, 1–30.

Melander, M. V. & Hussain, F. 1993 Polarized vorticity dynamics on a vortex column. *Phys. Fluids* A **5**, 1992–2003.

Melander, M. V. & Hussain, F. 1994 Core dynamics on a vortex column. *Fluid Dyn. Res.* **13**, 1–37.

Miyazaki, T. & Hunt, J. C. R. 1998 Turbulence structure around a columnar vortex – RDT and vortex wave excitation. In *Advances in Turbulence VII* (ed. U. Frisch) pp. 373–376. Kluwer.

Moore, D. W. & Saffman, P. G. 1972 The motion of a vortex filament with axial flow. *Phil. Trans. R. Soc. Lond.* A **272**, 407–429.

Passot, T., Politano, H., Sulem, P.-L., Angilella, J. R. & Meneguzzi, M. 1995 Instability of strained vortex layers and vortex tube formation in homogeneous turbulence. *J. Fluid Mech.* **282**, 313–338.

Saffman, P. G. 1992 *Vortex Dynamics*, pp. 241–252. Cambridge University Press.

Schoppa, W., Hussain, F. & Metcalfe, R. W. 1995 A new mechanism of small-scale transition in the plane mixing-layer: core dynamics of spanwise vortices. *J. Fluid Mech.* **298**, 23–80.

Siggia, E. D. 1981 Numerical study of small scale intermittency in three-dimensional turbulence. *J. Fluid Mech.* **107**, 375–406.

Verzicco, R., Jiménez, J. & Orlandi, P. 1995 On steady columnar vortices under local compression. *J. Fluid Mech.* **299**, 367–387 (referred to herein as VJO).

Verzicco, R. & Orlandi, P. 1996 A finite-difference scheme for three-dimensional incompressible flows in cylindrical coordinates. *J. Comput. Phys.* **123**, 402–414.

Villasenor, J. & Vincent, A. 1992 An algorithm for the space recognition and time tracking of vorticity tubes in turbulence. *CVGIP: Image Understanding* **55**, 27–35.

Villermaux, E., Sixou, B. & Gagne, Y. 1995 Intense vortical structures in grid generated turbulence. *Phys. Fluids* **7**, 2008–2013.

Vincent, A. & Meneguzzi, M. 1991 The spatial structure and statistical properties of homogeneous turbulence. *J. Fluid Mech.* **225**, 1–25.

Vincent, A. & Meneguzzi, M. 1994 On the dynamics of vorticity tubes in homogeneous turbulence. *J. Fluid Mech.* **258**, 245–254.